

# Systematic Design of Superprism-Based Photonic Crystal Demultiplexers

Babak Momeni, *Student Member, IEEE*, and Ali Adibi, *Senior Member, IEEE*

**Abstract**—In this paper, design of photonic crystal demultiplexers based on superprism effect is discussed. Figures of merit for performance of these demultiplexers are defined and a systematic design procedure is presented. We consider different design schemes, based on equal angular separation between channels and equal frequency separation between channels, and find the optimum structures among conventional photonic crystal lattices for each case. Our results provide design solutions for a range of current applications.

**Index Terms**—Demultiplexer, photonic crystal, superprism.

## I. INTRODUCTION

SINCE THE introduction of photonic crystals (PCs) [1], [2], a lot of interest toward these periodic structures has been motivated by recognizing the ability to control their photonic bandgap, i.e., a range of frequencies with no allowed electromagnetic modes. This photonic bandgap has been effectively used to realize photon localization, guiding, and suppressing spontaneous emission [1]–[5]. On the other hand, exploiting properties of wave propagation inside PCs has been addressed only recently.

After Lin *et al.* [6] proposed the effective prism structure using PC synthetic materials, the idea of superprism phenomenon has been developed [7]–[9] and assessed [10], [11] for wavelength demultiplexing in PCs. This idea has been implemented in one-dimensional (1-D) and two-dimensional (2-D) planar PCs [12]–[14], which show different spatial distributions of the light for different wavelength channels at the output. Some modifications to the PC lattice for improving the demultiplexing properties of the PC structures have also been proposed [15]. The systematic design of superprism-based PC demultiplexers for different applications, however, to our knowledge has not been addressed to date. The motivation behind this type of demultiplexers is their compactness and possibility of integration with other PC devices on a single substrate, which makes them a potential candidate for optical communication systems, spectroscopy, and sensing.

In order to effectively exploit demultiplexing capability of PCs in different applications, a few basic steps are necessary. First, we should have an understanding of the physical concepts of the effect, including dispersive behavior of PCs and wave

propagation behavior inside PCs. Second, a meaningful measure for the performance of the device has to be defined based on our design goals. Finally, we should be able to systematically design structure parameters to get our desired behavior. We cover these issues in this paper and present a design strategy that can be used to realize a demultiplexer based on wavelength separation properties of PCs for different applications.

Our analysis is based on an approximate model to describe the diffraction of optical beams in PCs [16]. We use this model to derive basic properties needed for designing demultiplexers, which are divergence angle of each beam inside the PC, crosstalk between adjacent beams (corresponding to adjacent wavelength channels), and the required propagation length to achieve acceptable spatial separation of different wavelength channels. Then, we will define practical measures to be used as useful criteria for comparing different structures and will use these measures to find the optimum design parameters for each case. Note that these measures can differ from one application to another. In most practical applications, there are two main design modes that we are interested in: 1) spatially separating a range of wavelengths without strong constraints on each channel frequency or the separation between the adjacent channels (as in spectroscopic applications), and 2) separating channels with assigned equal frequency separation (which is of interest in WDM applications). In this paper, we consider these two cases and define performance measures for each case. In Section II, we provide the basic background, as well as an introduction to the effective index model, which will be used throughout the paper for describing beam propagation inside PCs. In Section III, figures of merit for different schemes are defined and calculated as functions of different design parameters in a superprism demultiplexer structure. Optimization scheme and the optimum structures for different cases are presented and discussed in Section IV. A unified design process for conventional superprism-based demultiplexers is presented in Section V. Section VI includes some implementation issues that need to be considered in a practical design. Final conclusions are made in Section VII.

## II. THEORETICAL BACKGROUND

The geometry of the demultiplexing structures we consider in this paper is schematically shown in Fig. 1. We assume that the incident beam is a Gaussian beam which is incident from a homogeneous and isotropic material with refractive index  $n_1$  on the 2-D PC structure at an incident angle  $\alpha$  and has a divergence angle  $\Delta\alpha$ . The ultimate goal of demultiplexing is to separate different wavelength channels (which are assumed to be narrowband centered at assigned frequencies) in space at the

Manuscript received June 29, 2004. This work was supported in part by the Air Force Office of Scientific Research (G. Pomrenke) and in part by the National Science Foundation (F. Bartoli).

The authors are with the School of Electrical and Computer Engineering, Georgia Institute of Technology, Atlanta, GA 30332-0250 USA (e-mail: momeni@ece.gatech.edu; adibi@ece.gatech.edu).

Digital Object Identifier 10.1109/JSAC.2005.851191

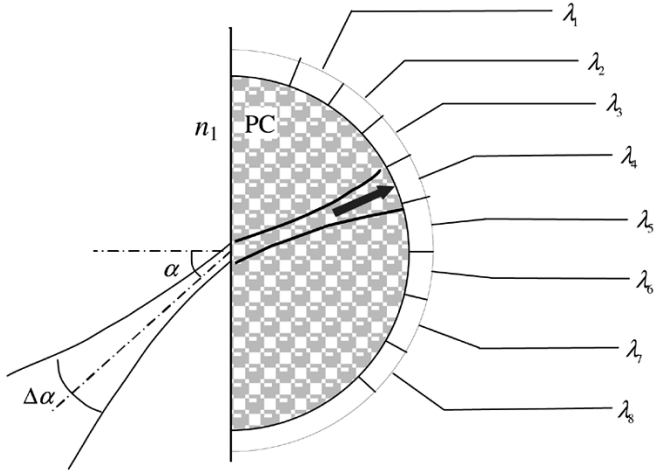


Fig. 1. Geometry of the superprism demultiplexers considered throughout this paper is schematically shown.  $\alpha$  is the angle of incident,  $\Delta\alpha$  is the divergence angle of the input beam, and the incident optical beam launches on the PC from a homogeneous region with refractive index  $n_1$ .

output. In order to analyze this structure, we first need to consider the propagation of each optical beam at a given frequency and angle of incident inside the PC. The propagation of an incident monochromatic plane wave inside the PC is well-understood based on group velocity of corresponding PC mode [17]. In practical realizations, however, the incident optical beam is not simply a plane wave and contains a range of wavevectors, as shown in Fig. 1. For such a nonplane-wave incident beam, we can still expand the incident field over its plane wave components and monitor the behavior of the corresponding propagating PC mode excited by each incident plane wave. Using this technique, we recently showed that under certain conditions (which are usually satisfied in practical devices), an effective index can be defined for the diffraction of a beam with each specific frequency and direction inside the PC [16], [18]. In terms of the parameters of the incident excitation, this effective index is given by [16], [18]

$$n_e(\alpha, \omega) = \frac{n_1 \cos \alpha}{(\partial \theta_g / \partial \alpha) |_{\omega} \cos \theta_g} \quad (1)$$

where  $\theta_g$  is the angle of group velocity (defined with respect to the normal to the interface) for the PC mode excited by a plane wave at frequency  $\omega$  and incident at an angle  $\alpha$  from a homogeneous medium with refractive index  $n_1$ . Note that  $\theta_g$  and its derivative as given in (1) are well-defined using the PC band structure at the frequency of operation. Using this simplified model, it can be shown that a Gaussian incident beam remains Gaussian inside the PC and all of its behavior can be modeled using the single effective index as given above [18]. It should be emphasized that this effective index can be used only to represent diffraction (and propagation) properties of the envelope of the beam propagating inside the PC and depends on both direction and frequency. This model cannot be used to analyze the reflection at the interface of the PC and the incident medium since the model relies on dispersion properties of propagating PC modes, and it does not consider evanescent modes at the boundary. Different techniques have been proposed to reduce the reflection at the interface of such structures [19]–[21],

and they can be adopted for the interface of the demultiplexing structure. Thus, in this paper, we only concentrate on the spatial demultiplexing properties of the PC structures caused by propagation through the periodic medium. In this paper, only spatial distribution of beams is of interest, and for this purpose the simplified effective index model suffices to represent the PC structure.

In order to calculate  $n_e(\alpha, \omega)$  corresponding to all plane wave components of the incident beam, we first calculate the direction of group velocity (or  $\theta_g$  in (1)) for each incident plane wave. This is done by calculating the band structure of the PC using plane wave expansion method, as described in [22]. For each point (or mode) in the band structure (given by frequency  $\omega$  and propagation vector), the direction of Poynting vector (perpendicular to the constant frequency contour at that point) is the same as the direction of group velocity for that mode inside the structure. We can numerically calculate the direction of group velocity from the band structure using [23]

$$\bar{v}_g = \nabla_{\bar{k}} \omega \quad (2)$$

where  $\bar{v}_g$ ,  $\bar{k}$ , and  $\nabla$  correspond to group velocity vector, propagation vector (or wavevector), and the gradient operator, respectively. By calculating the constrained derivative of the angle of group velocity along the constant frequency contours and using (1), we can find corresponding effective index of the beam propagating inside the PC region.

The divergence angle of the beam inside the PC is given by [11]

$$\delta = \left( \frac{\partial \theta_g}{\partial \alpha} \right) \Big|_{\omega} (\Delta \alpha). \quad (3)$$

Having the effective index and the divergence angle of the beam inside the PC, we can completely characterize the beam propagating in this region [18]. Note that the difference between  $\theta_g$  (as found from the PC band structure) for different wavelength channels is the primary mechanism used for wavelength demultiplexing in PCs. Also, beam divergence angles for different frequency channels inside the PC are generally different [as given by (3)] from each other, and the evolution of the beams at different frequency channels during propagation depend on their corresponding effective indices.

The relative extent of two adjacent wavelength channels inside the PC is schematically shown in Fig. 2(a), assuming that the two adjacent channels have equal divergence angles  $\delta$ . The overlap of the two beams depends on both the angular separation between these channels and the propagation length inside the PC. We define the crosstalk between channels as the total power of each channel at the position of other channels. Assuming the beams inside the PC to be Gaussian (which is justified for a Gaussian incident beam, as shown in [18]), and the angular separation between the two adjacent channels (calculated at their center frequencies) to be  $\Theta$ , the propagation length required to limit crosstalk to a desired value  $X$  is found approximately as

$$\begin{cases} L(X) = \zeta(X) z_0 \\ \zeta(X) = \frac{K(X)}{\eta - H(X)} \end{cases} \quad (4)$$

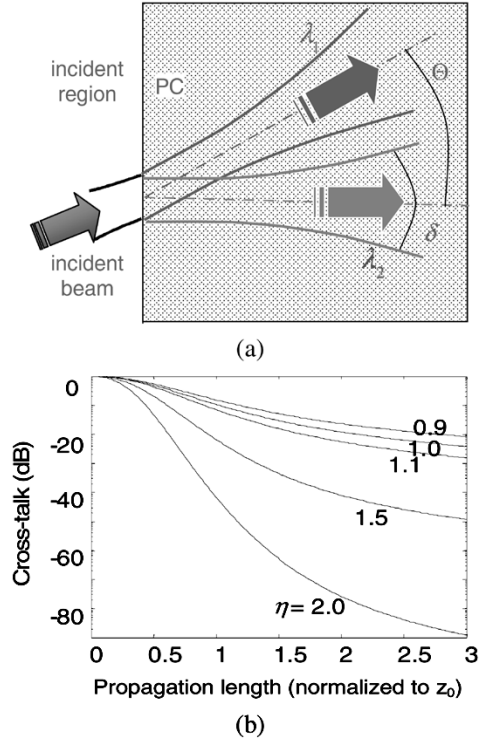


Fig. 2. (a) Schematic evolution of beam profiles of two adjacent wavelength channels inside the PC structure.  $\Theta$  is the angular spacing between group velocity directions of center frequencies of these two channels, and  $\delta$  is the divergence angle of one channel inside the PC region. (b) The behavior of crosstalk versus propagation length for different values of  $\eta = \Theta/\delta$ . Gaussian beam approximation is used in all cases.

TABLE I  
CROSSTALK PARAMETERS

Crosstalk, $X$ (dB)	$K(X)$	$H(X)$
-20	0.9	0.56
-30	0.9	0.83
-40	0.9	1.04
-50	0.9	1.22

where  $z_0 = 4\lambda_0/(\pi n_e \delta^2)$  is the Rayleigh range for the beam,  $\lambda_0$  is the free-space wavelength, and  $\eta = \Theta/\delta$  is the angular separation factor. Equation (4) is found by interpolating the simulated data. The coefficients  $K(X)$  and  $H(X)$  in (4) depend only on the crosstalk  $X$ , and not on other design parameters; their values are listed in Table I. In order to find  $K(X)$  and  $H(X)$ , we calculated crosstalk (assuming Gaussian beams) for several different device lengths ( $L$ ) and design parameters  $\Theta/\delta$ . A subset of the results appears in Fig. 2(b), which shows the variations of crosstalk versus propagation length for different angular separation factors,  $\eta$ . We then fitted the data to (4) to obtain values of  $K(X)$  and  $H(X)$  for each value of crosstalk,  $X$ . The error in this curve fitting for all cases in the range of interest was less than 5%. Since the propagation inside the PC is modeled using the effective index technique, the results in Fig. 2(b) and Table I are independent of the choice of PC. The importance of this equation is in that it relates the required propagation length

$L$  (which is directly related to the physical size of the demultiplexer) to other parameters (i.e., beam divergence,  $\delta$ , and angular separation between channels  $\Theta$ ) based on the acceptable crosstalk level.

Now, we have enough tools to define the design of a PC demultiplexer based on superprism effect as a well-posed problem. As mentioned earlier, there are two basic types of structures in demultiplexing applications, in one case, we want to separate the incident wavelength channels into equally spaced angles [we call it equal angular spacing scheme (EAS)], and in the other case, channels should be equally spaced in frequency [equal frequency spacing scheme (EFS)]. For each of these cases, we need appropriate measures to assess the demultiplexing performance of the structures and to find the optimum structure.

### III. FIGURES OF MERIT FOR PC DEMULTIPLEXERS

In this section, we define the main figures of merit for the performance of different types of PC demultiplexer. The two primary merits for the performance of these structures that we consider here are compactness of the structure and divergence angle requirement for the incident (or input) beam. Compactness is one of the main advantages of the superprism-based demultiplexers and an optimum design must result in as compact a structure as possible. The smaller the area of the structure is, the higher the yield; the lower the cost; and the less the complications due to the nonuniformity of the structure would be. Moreover, scattering loss, which is still one of the major issues in planar PC structures, increases as the size of the structure is increased. On the other hand, in order to avoid huge crosstalk and realize spatial separation of channels in a PC structure with reasonable size (or alternatively, to achieve the desired resolution [10]), some limitations must be imposed on the divergence angle of the incident beam. It is practically difficult to launch very large beam sizes with very small divergence angles into the planar PC structure. Designing structures that can effectively work with incident beams with reasonable divergence angles ( $\Delta\alpha$  in Fig. 1) is essential for realizing practical PC demultiplexers. Therefore, compactness and incident divergence angle are considered here as the main features for which figures of merit are defined.

The physical area is a reasonable measure for the compactness of a PC demultiplexer. If the minimum propagation length for achieving the required crosstalk level ( $X$ ) and the total angular range of operation over which all separated wavelength channels exist inside the PC are represented by  $L$  and  $\theta_T$ , respectively, the area of the structure will be

$$A = \frac{1}{2}\theta_T L^2 \cong \frac{\theta_T}{2} \left( \max_{\text{channels}} \left\{ \frac{4\zeta(X)\lambda}{\pi n_e \delta^2} \right\} \right)^2. \quad (5)$$

Note that the required propagation lengths for different channels are in general different. For calculating the area of the structure, the worst case (i.e., the channels with largest propagation length) must be considered. Thus, we can use (4) to define  $L$  as

$$L \cong \max_{\text{channels}} \left\{ \frac{4\zeta(X)\lambda}{\pi n_e \delta^2} \right\} \quad (6)$$

where  $\max_{\text{channels}}$  refers to maximum value over all wavelength channels in the demultiplexer. Using (1) and (5), we obtain

$$A \cong \frac{8\lambda^2\theta_T}{\pi^2} \left( \max_{\text{channels}} \left\{ \left( \frac{K}{\eta - H} \right) \frac{(\partial\theta_g/\partial\alpha)|_{\omega} \cos\theta_g}{n_1 \cos\alpha\delta^2} \right\} \right)^2 \quad (7)$$

in which  $X$ -dependence in  $K = K(X)$  and  $H = H(X)$  is implicit. Using  $\eta = \Theta/\delta$ , we can simplify  $A$  to

$$A \cong \frac{8\lambda^2 K^2 \theta_T}{n_1^2 \pi^2 \cos^2 \alpha} \left( \max_{\text{channels}} \left\{ \frac{(\partial\theta_g/\partial\alpha)|_{\omega} \cos\theta_g}{(\Theta - H\delta)\delta} \right\} \right)^2. \quad (8)$$

Combining (3) and (8), we get

$$A \cong \frac{8\lambda^2 K^2 \theta_T}{n_1^2 \pi^2 \cos^2 \alpha} \left( \frac{1}{\Delta\alpha} \right)^2 \times \left( \max_{\text{channels}} \left\{ \frac{\cos\theta_g}{\Theta - H(\partial\theta_g/\partial\alpha)|_{\omega} \Delta\alpha} \right\} \right)^2 \quad (9)$$

where  $(\partial\theta_g/\partial\alpha)|_{\omega}$ ,  $\cos\theta_g$ , and  $\Theta$  are the values corresponding to each channel, and the maximum value is obtained over all channels. Now, we consider equal angular separation (EAS) and equal frequency separation (EFS) demultiplexing schemes separately for further derivations.

1) *Equal Angular Separation With Flexible Frequencies (EASFF)*: In this case,  $\Theta$  has to be chosen for the worst channels (the largest value) and is the same for all channels. For design purposes, the regions in the PC band structure with smaller values for  $(\partial\theta_g/\partial\alpha)|_{\omega}$  are advantageous for this scheme. If we limit this value to a threshold  $\beta$  (i.e.,  $(\partial\theta_g/\partial\alpha)|_{\omega} < \beta$ ) as discussed in [11], then

$$A \cong \frac{8\lambda^2 K^2 \theta_T(\alpha, \beta)}{n_1^2 \pi^2 \cos^2 \alpha} \left( \frac{1}{\Delta\alpha} \right)^2 \left( \max_{\text{channels}} \left\{ \frac{\cos\theta_g}{\Theta - H\beta\Delta\alpha} \right\} \right)^2. \quad (10)$$

Using simple calculus, it can be shown that the area  $A$  is minimized by setting  $\Delta\alpha = \Theta/(2H\beta)$ , which results in

$$A \cong \frac{8\lambda^2 K^2 \theta_T}{n_1^2 \pi^2 \cos^2 \alpha} \left( \frac{4H^2\beta^2}{\Theta^2} \right) \left( \frac{4\cos^2\theta_g}{\Theta^2} \right) \quad (11)$$

where  $\theta_{\text{gm}}$  is the propagation angle in the range of interest which maximizes  $\cos^2\theta_g$ . For  $N$  demultiplexed channels,  $\theta_T = N\Theta$ , thus

$$A \cong \frac{128\lambda^2 K^2 H^2}{n_1^2 \pi^2} \frac{\beta^2 \cos^2\theta_{\text{gm}}}{\theta_T^3(\alpha, \beta) \cos^2\alpha} N^4. \quad (12)$$

This basically tells us that in these demultiplexers the area of the structure is proportional to the fourth power of the number of channels. The coefficient of this relation can be defined as the compactness factor  $C$  with

$$C_{\text{EASFF}} = \left( \frac{n_1^2 \pi^2}{128 K^2 H^2} \frac{\theta_T^3(\alpha, \beta) \cos^2\alpha}{\beta^2 \cos^2\theta_{\text{gm}}} \right); \quad \frac{A}{\lambda^2} \cong \frac{N^4}{C_{\text{EASFF}}}. \quad (13)$$

Compactness factor, as defined in (13), depends on the PC structure (through  $\theta_T$ ), and on the parameters  $\alpha$  and  $\beta$ . In order to realize an  $N$ -channel demultiplexer in this scheme, the larger the compactness factor is, the more compact the structure will be. Therefore,  $C_{\text{EASFF}}$  can be used as a measure of compactness of the structure to compare different designs. In the process of minimizing the area of the structure, we obtained

$$\Delta\alpha = \Theta/(2H\beta). \quad (14)$$

Rearranging this formula using  $\theta_T = N\Theta$ , we get

$$\Delta\alpha = \frac{\theta_T(\alpha, \beta)}{2H\beta} \frac{1}{N} \quad (15)$$

which means that for a given design in this scheme the required incident divergence angle decreases as the number of channels increases. Reducing the incident divergence angle usually requires more sophisticated optical design; therefore, a design with less strict requirement for the divergence angle of input beam is more favorable. We define the other performance measure (which depends on both the PC and the design parameters) as incident divergence factor  $E_{\text{EASFF}}$ , where

$$E_{\text{EASFF}} = \frac{\theta_T(\alpha, \beta)}{2H\beta}; \quad \Delta\alpha = \frac{E_{\text{EASFF}}}{N}. \quad (16)$$

In optimizing PC structures for EASFF scheme, we use  $C_{\text{EASFF}}$  and  $E_{\text{EASFF}}$  as the two main figures of merit. The values of  $C_{\text{EASFF}}$  and  $E_{\text{EASFF}}$  depend on  $\alpha$  and  $\beta$  and maximizing a goal function based on  $C_{\text{EASFF}}$  and  $E_{\text{EASFF}}$  requires an optimization over  $(\alpha, \beta)$  plane. Once the optimization is complete, the corresponding values  $\alpha_{\text{opt}}$ ,  $\beta_{\text{opt}}$ , and  $\theta_{T,\text{opt}}$  for the optimum structure are known, and for desired number of channels  $N$ , the design parameters can be found as

$$\Delta\alpha = \frac{\theta_{T,\text{opt}}}{2H\beta_{\text{opt}}N} = \frac{E_{\text{EASFF}}}{N} \quad (17)$$

$$L = \lambda \left( \frac{C_{\text{EASFF}} \theta_{T,\text{opt}}}{2} \right)^{-1/2} N^2. \quad (18)$$

2) *Equal Angular Separation With Specified Frequencies (EASSF)*: The main difference here, compared with the flexible frequency scheme, is that the frequency range of operation of the device is given. In applications such as spectroscopy, one of the main performance measures for the demultiplexer is the frequency resolution (i.e., how close the frequencies that it can resolve are located with respect to each other). Knowing the number of channels by itself does not express the resolution since it has no information about the distribution of channels in frequency. For a single channel, normalized resolution can be defined as center frequency of the channel ( $\omega_j$ ) divided by frequency separation of that channel from its adjacent channels ( $\Delta\omega_j$ ); i.e.,  $\omega_j/\Delta\omega_j$  for  $j$ th channel. For a demultiplexer with multiple arbitrarily spaced channels, we need to combine these individual normalized resolutions ( $\omega_j/\Delta\omega_j$ ) to obtain a reasonable performance measure that can be used to compare different designs. In order to represent the performance over the

entire spectrum of operation, we define the resolution measure  $R$  as

$$R = \sum_{\text{channels}(j)} \frac{\omega_j}{\Delta\omega_j}. \quad (19)$$

This parameter, the frequency resolution (or resolution) of the device, is considered here as a measure of performance for the demultiplexer. We use an averaged version of the resolution to reflect the behavior in the entire frequency range of interest. Assuming that the device is designed for a specified frequency range  $\Omega$ , then

$$R = N \left( \frac{\omega_0}{\Delta\omega} \right)_{\text{avg}} \cong N \frac{\omega_0 \int_{\Omega} (1/\Delta\omega) d\omega}{\int_{\Omega} d\omega}. \quad (20)$$

The size of the structure is another performance measure of interest in this case as well. We will use the resolution per unit area as our figure of merit for the following discussions. Having equal angular separation ( $\Theta$ ) between channels results in

$$\frac{1}{(\Delta\omega)_j} = \left( \frac{\partial\theta_g}{\partial\omega} \right) \Big|_{\alpha,j} \frac{1}{\Theta} \quad (21)$$

where  $(\partial\theta_g/\partial\omega)|_{\alpha,j}$  and  $(\Delta\omega)_j$  are the values corresponding to each channel ( $j = 1, \dots, N$ ). Hence, the normalized resolution per device area is defined using (10), (20), and (21) as

$$R_n = \frac{R\lambda^2}{A} = \frac{n_1^2\pi^2 \cos^2 \alpha}{8K^2} \frac{N\omega_0 \int_{\Omega} (\partial\theta_g/\partial\omega)|_{\alpha} d\omega}{\omega_T \theta_T \Theta} \times (\min\{\Theta - H(\partial\theta_g/\partial\alpha)|_{\omega} \Delta\alpha\})^2 (\Delta\alpha)^2. \quad (22)$$

Similar to the EASFF case,  $R_n$  can be maximized by setting

$$\Delta\alpha = \frac{\Theta}{2H \max_{\Omega} (\partial\theta_g/\partial\alpha)|_{\omega}} = \frac{\theta_T}{2H \max_{\Omega} (\partial\theta_g/\partial\alpha)|_{\omega} N} \quad (23)$$

which results in

$$R_n = \frac{n_1^2\pi^2}{128K^2H^2} \frac{\omega_0\theta_T^3 \cos^2 \alpha}{\omega_T (\max_{\Omega} \{(\partial\theta_g/\partial\alpha)|_{\omega}\})^2 N^2}. \quad (24)$$

From this relation, it can be observed that the resolution per unit area decreases as the second power of number of channels ( $N$ ) in this scheme.

We can define the resolution factor as

$$\rho_{\omega} = \frac{n_1^2\pi^2}{128K^2H^2} \frac{\omega_0\theta_T^3 \cos^2 \alpha}{\omega_T (\max_{\Omega} \{(\partial\theta_g/\partial\alpha)|_{\omega}\})^2}; \quad R_n = \frac{\rho_{\omega}}{N^2} \quad (25)$$

and this value  $\rho_{\omega}$ , will be used as the main figure of merit in our designs.

3) *Equal Frequency Separation With Specified Frequencies (EFSFF)*: In this case, the frequency separation between adjacent channels is equal. An example for this case is a DWDM wavelength demultiplexer. The incident divergence angle can be found as

$$\Delta\alpha = \gamma \frac{\Delta\omega}{2H} \quad (26)$$

with

$$\gamma = \min_{\text{channels}} \left\{ \frac{(\partial\theta_g/\partial\omega)|_{\alpha}}{(\partial\theta_g/\partial\alpha)|_{\omega}} \right\} \quad (27)$$

in which the minimum value is obtained over all wavelength channels in the frequency range of interest. Using (9) along with  $\Theta = (\partial\theta_g/\partial\omega)|_{\alpha} \Delta\omega$  for each channel, the area of the structure is

$$A \cong \frac{8\lambda^2 K^2 \theta_T}{n_1^2 \pi^2 \cos^2 \alpha} \left( \frac{2H}{(\Delta\omega)^2} \right)^2 \gamma^{-2} \times \max_{\text{channels}} \left\{ \frac{\cos \theta_g}{(\partial\theta_g/\partial\omega)|_{\alpha} - \frac{1}{2}(\partial\theta_g/\partial\alpha)|_{\omega} \gamma} \right\}^2. \quad (28)$$

Using  $\omega_T = N\Delta\omega$ , we obtain

$$A \cong \frac{32\lambda^2 K^2 H^2}{n_1^2 \pi^2 \cos^2 \alpha} \left( \frac{\theta_T}{\omega_T^4} \right) \gamma^{-2} \times \max_{\text{channels}} \left\{ \frac{\cos \theta_g}{(\partial\theta_g/\partial\omega)|_{\alpha} - \frac{1}{2}(\partial\theta_g/\partial\alpha)|_{\omega} \gamma} \right\}^2 N^4 \quad (29)$$

where  $\omega_T$  is the total bandwidth of the designed device. The same behavior as in EASFF scheme can be seen here, in which the area of the structure increases as the fourth power of the number of channels. Similar to the EASFF case, we can define compactness factor as

$$C_{\text{EFSFF}} = \frac{n_1^2\pi^2}{128K^2H^2} \frac{\omega_T^4 \gamma^2 \cos^2 \alpha}{\theta_T} \times \min_{\text{channels}} \left\{ \frac{(\partial\theta_g/\partial\omega)|_{\alpha} - \frac{\gamma}{2}(\partial\theta_g/\partial\alpha)|_{\omega}}{\cos \theta_g} \right\}^2; \quad \frac{A}{\lambda^2} \cong \frac{N^4}{C_{\text{EFSFF}}} \quad (30)$$

and the incident divergence factor as

$$E_{\text{EFSFF}} = \frac{\omega_T \gamma}{2H}; \quad \Delta\alpha = \frac{E_{\text{EFSFF}}}{N}. \quad (31)$$

The quantities  $C_{\text{EFSFF}}$  and  $E_{\text{EFSFF}}$  are considered as the figures of merit for superprism-based PC demultiplexers in this scheme.

#### IV. RESULTS AND DISCUSSION

In all simulations of this section, we assume that the 2-D PC structure is formed by etching a periodic lattice of air-holes in a Si substrate. The incident beam is assumed to have a Gaussian spatial profile incident from a homogeneous Si region onto the interface with the PC. In order to comply with practical fabrication limitations, we only consider the values of  $r/a$  ( $r$  being the radius of holes, and  $a$  being the lattice constant) between 0.2 and 0.4. The interface of the PC with the homogeneous Si region is always chosen along a high-symmetry direction of the lattice. We first consider a demultiplexer with flexible frequencies in equal angular separation scheme (EASFF). We define our optimization goal in this case to be  $G = (C_{\text{EASFF}})^2 E_{\text{EASFF}}$  having more emphasis on the size of the structure. For each PC lattice (i.e., square, triangular, etc.), we vary  $r/a$  to search for

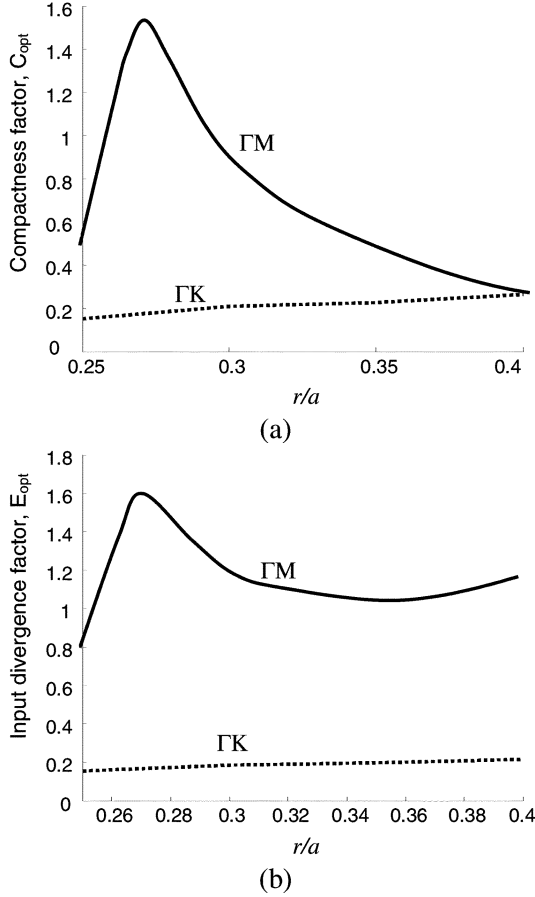


Fig. 3. (a) Optimal compactness factor and (b) optimal input divergence factor are shown for various radiuses of holes in a 2-D triangular lattice PC of air-holes inside Si. Optimization in each case is performed for the goal function  $G = C_{EASFF}^2 E_{EASFF}$ . Solid lines and dotted lines correspond to the structure with interface parallel to  $\Gamma M$  and  $\Gamma K$  directions, respectively. These results are obtained by curve fitting into actual optimization data.

TABLE II  
RESULTS OF OPTIMIZATION (OVER  $\alpha$ ,  $\omega_{n0}$ , AND RADIUS) IN EASSF SCHEME

Lattice type	Pol.	$r/a$	$\alpha_{opt}$	$\beta_{opt}$	$\theta_{r,opt}$	$C_{opt}$	$G_{opt}$
Square	TE	0.35	16°	2.75	19.4°	0.017	3.5e-5
	TM	0.30	14°	2.44	22.1°	0.032	1.6e-4
Triangular ( $\Gamma M$ )	TE	0.27	9°	0.11	10.0°	1.56	3.94
	TM	0.20	4°	1.96	21.4°	0.047	4.3e-4
Triangular ( $\Gamma K$ )	TE	0.40	8°	7.5	92.8°	0.26	1.5e-2
	TM	0.40	4°	16	90.7°	0.054	3.0e-4

the best demultiplexing behavior. Results of this search for triangular lattice PCs with interface parallel to  $\Gamma M$  and  $\Gamma K$  directions and TE polarization are shown in Fig. 3. The results of optimization for different structures are given in Table II. These results are obtained by finding the optimum structure (using  $G = (C_{EASFF})^2 E_{EASFF}$  as the goal function) for each lattice type, interface direction, and polarization when all values of  $\alpha$ ,  $\beta$ , and  $(r/a)$  are searched. Note that in each case, scaling the structure by an appropriate factor can be used to set the operation wavelength to our desired value.

It can be seen from Table II that if no other limitation is involved, the triangular lattice PC with interface parallel to the  $\Gamma M$  direction can provide demultiplexers with at least two orders of

TABLE III  
RESULTS OF OPTIMIZATION (OVER  $\alpha$ ,  $\omega_{n0}$ , AND RADIUS) IN EASSF SCHEME WITH 5% DEMULTIPLEXING BANDWIDTH

Lattice type	Pol.	$r/a$	$\alpha_{opt}$	$\omega_{n,opt}$	$\beta_{opt}$	$\theta_{r,opt}$	$\rho_{opt}$
Square	TE	0.35	24°	0.2412	2.2	15°	0.22
	TM	0.30	20°	0.2494	2.7	22°	0.50
Triangular ( $\Gamma M$ )	TE	0.30	10°	0.2380	0.04	2.8°	4.8
	TM	0.20	46°	0.2306	21	70°	0.14
Triangular ( $\Gamma K$ )	TE	0.35	8°	0.2099	1.1	12°	0.48
	TM	0.35	4°	0.2386	20	69°	0.30

magnitude better performance compared with other lattices (at the same number of channels). Note that in this region the divergence factor  $\beta$  (and therefore, divergence of the beam inside the PC region), is very small and structure is being used in supercollimation regime [24]. For small number of channels, however, a degradation factor has to be taken into account for these devices, and the values in Table II are not exact. The reason is that for small  $N$  in (16), the divergence angle is relatively large which means the spatial bandwidth of the signal is large and a considerable portion of the band structure is excited by the incident beam. The quadratic approximation for the band structure (i.e., the assumption for effective index model [18]) may not be valid for such large spatial bandwidths and broadening due to higher order terms of the band structure expansion needs to be considered for a more precise treatment. However, the structure with small  $N$  is usually not the desired case for practical applications.

Note that the number of channels does not appear specifically in Table II. However, for every desired number of channels ( $N$ ), we can use (13) and (16) to find the required size of the structure as well as the required divergence angle. The values in Table II can be used to obtain quickly an estimate about how large the corresponding demultiplexing structure is. For instance, using a triangular lattice PC with  $r/a = 0.27$  and TE polarization, a 64-channel demultiplexer has an approximate area of  $A \approx 64^4 \lambda^2 / 1.56 \approx 1.1 \times 10^7 \lambda^2$ , which is 26 mm<sup>2</sup> at 1.55  $\mu m$  operation wavelength.

For EASSF scheme, we use the same procedure (with  $\rho_{EASSF}$  as optimization goal) and optimize the structure. Design parameters used in optimization in this case are the center frequency of the device ( $\omega_0$ ), polarization of the input beam, direction of the boundary with respect to PC high-symmetry directions, incident angle ( $\alpha$ ), and  $(r/a)$  for the lattice. The results of optimization for a 5% bandwidth (i.e.,  $\omega_T = 0.05\omega_0$ ) are shown in Table III. The results in Table III show that the best performance for EASSF scheme is obtained using TE polarization in a triangular lattice PC with boundary along  $\Gamma M$  direction with at least one order of magnitude better performance compared with other structures.

Similar steps can be followed for EFSSF scheme with  $C_{EFSSF}$  and  $E_{EFSSF}$  as merits, and  $G = (C_{EFSSF})^2 E_{EFSSF}$  as the goal function. We assume a bandwidth of 5% for these demultiplexers, and search over all the point in the first Brillouin zone. The results are shown in Table IV, which show that for these conditions, triangular lattice with TE polarization with boundary along  $\Gamma M$  direction delivers the best performance among the listed choices with at least two orders of magnitude better performance compared with other structures. These

TABLE IV  
RESULTS OF OPTIMIZATION (OVER  $\alpha$ ,  $\omega_{n0}$ , AND RADIUS) IN EFSSF SCHEME  
WITH 5% DEMULTIPLEXING BANDWIDTH

Lattice type	Pol.	$r/a$	$\alpha_{opt}$	$\omega_{n,opt}$	$\theta_{T,opt}$	$C_{opt}$	$G_{opt}$
Square	TE	0.35	26°	0.2396	25.8°	0.056	3.6e-4
	TM	0.27	24°	0.2354	31.6°	0.12	4.1e-3
Triangular (TM)	TE	0.30	10°	0.2355	3.0°	0.71	4.2e-1
	TM	0.40	18°	0.4651	9.8°	0.007	8.0e-6
Triangular (TK)	TE	0.32	8°	0.2305	10.2°	0.038	4.8e-4
	TM	0.20	16°	0.2525	112°	0.042	8.0e-5

results can also be used to obtain an estimate of the size of the structure. For example, for  $N = 16$  channels at  $\lambda = 1550$  nm with 5% overall bandwidth (0.3125% relative channel spacing), the area of the structure is approximately  $0.22 \text{ mm}^2$ .

In general, in order to spatially separate the beams with different wavelengths inside the structure, the divergence of the beam inside the PC (and, therefore, the required divergence of the incident beam) should be limited to some extent. This restriction becomes more important as the angular or frequency separation between channels becomes smaller. This, along with the required propagation length being proportional to the Rayleigh range of the beam inside the PC [according to (4)] are the reasons for the area of the structure being proportional to the fourth power of number of channels in these devices.

Comparing to the relations presented in [10], our approach provides a more accurate description of propagation of beam inside periodic structures and extends the paraxial approximation given in [10] to a more general case. Also, in [10], the required propagation length to achieve spatial separation of channels is estimated to be the Rayleigh range of the beam. However, here we have shown that an extra factor  $\zeta(X)$  needs to be considered that depends on the crosstalk level, and angular separation between channels. In addition, we have provided a more rigorous optimization process (based on figures of merit for different design schemes) that results in design solutions for a range of practical applications.

## V. UNIFIED DESIGN PROCEDURE

Based on the results of the previous sections, we propose the following procedure for designing a superprism-based PC demultiplexer. First, according to the desired demultiplexing scheme, corresponding figures of merit are chosen and an appropriate goal function is defined. Second, the goal function is used to compare different PC structures and different points of band structure to find the best region of operation. This includes optimization over  $\alpha$  and  $\Delta\alpha$  in most cases. Finally, the local parameters (angle of group velocity, effective index, frequency, etc.) around the operation point are found and parameters are set to achieve the separation in space for different channels.

As design examples, assume a square lattice PC with TM polarization is chosen for the demultiplexer. First, consider a demultiplexer in the EASFF scheme. From Table II, the optimum design parameters are  $r/a = 0.30$  and  $\alpha = 14^\circ$  (boundary is along one of the basic lattice vectors) with  $\beta_{opt} = 2.44$ . The dependence of the angle of group velocity versus normalized frequency for this PC is shown in Fig. 4(a). It can be found

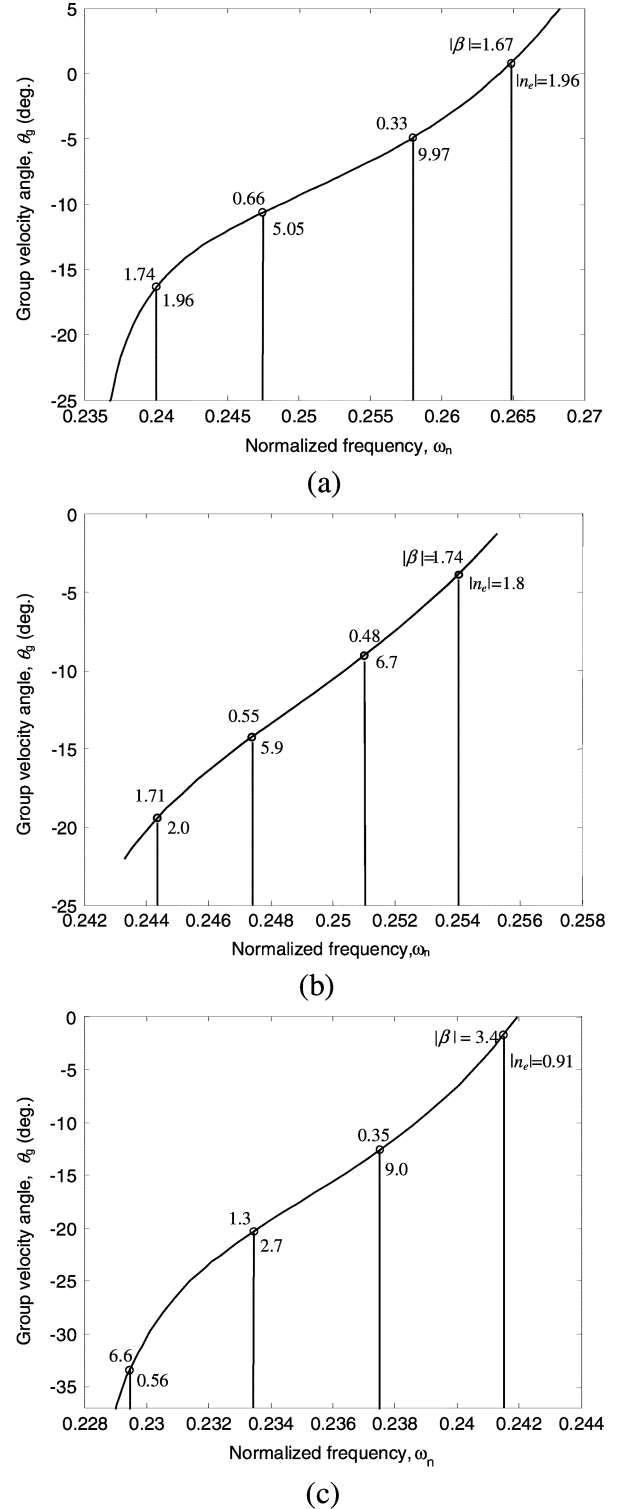


Fig. 4. Variations of the angle of group velocity versus normalized frequency for a square lattice PC with TM polarization are shown in optimal structures of three different schemes. (a) Normalized frequencies of channels are selected according to EASFF scheme (highlighted by circles). (b) Normalized frequencies of channels are selected according to EASSF scheme. (c) Normalized frequencies of channels are selected according to EFSSF scheme. The number above each channel shows the value of  $\partial\theta_g/\partial\alpha$  for that channel, and the number below it shows its corresponding value for the effective index.

from Fig. 4(a) that the angular spacing between adjacent channels (same as the angular separation between their group velocity directions) for  $X = -20$  dB in this case is  $\Theta = 5.6^\circ$ . For

this design at  $\lambda = 1.55 \mu\text{m}$ , we obtain a propagation length of  $L \approx 210 \mu\text{m}$  and an input divergence angle of  $\Delta\alpha = 3.2^\circ$ . As the second example, consider the same lattice type and polarization, but with a known 5% bandwidth for the demultiplexer in the EASSF scheme. According to Table IV, the best design for this case has  $r/a = 0.30$  and  $\alpha = 20^\circ$ . The curve for angle of group velocity versus normalized frequency and distribution of channels for this demultiplexer are shown in Fig. 4(b). From Fig. 4(b), the angular spacing between adjacent channels for  $X = -20 \text{ dB}$  is  $\Theta = 5.2^\circ$ . For this design at  $\lambda = 1.55 \mu\text{m}$ , we obtain a propagation length of  $L \approx 260 \mu\text{m}$  and an input divergence angle of  $\Delta\alpha = 3^\circ$ . Larger propagation length compared with the first example is due to the extra constraint of known demultiplexing bandwidth (It is worth to mention that the device designed in EASSF scheme has smaller area at the expense of lower resolution.) Note that in both these cases the channels are not distributed uniformly over frequency. Now, consider a four-channel demultiplexer with channels of equal frequency separation and with a known 5% bandwidth (EFSSF scheme). Using the same square lattice with TM polarization, the design parameters are obtained from Table III to be  $r/a = 0.27$  and  $\alpha = 24^\circ$  with normalized frequency of the device centered at  $\omega_n = 0.2354$ . Fig. 4(c) shows the variations of group velocity angle with frequency and location of frequency channels. The properties of the designed device are  $\Delta\alpha = 2.5^\circ$  and propagation length  $L \approx 240 \mu\text{m}$ . Comparing Fig. 4(a)–(c), it can be observed that the choices of angle of incident, properties of the lattice, and distribution of channels depend on the specific design scheme and using our figures of merit it is possible to design and optimize the demultiplexer for these three schemes.

Using the parameters in Fig. 4(a), we have performed a brute-force simulation (based on a combination of plane wave expansion and mode matching methods) to model the propagation of optical beams inside PC structures. The resulting field intensities at the output plane are shown in Fig. 5. It can be seen from Fig. 5 that separation of frequency channels in space is achieved, and results are consistent with those predicted by effective index model.

It should be emphasized that in the selection of the optimum structure, here, we have not considered the permittivity distribution in a unit cell of the PC (for example, by using noncircular holes) or other lattices. Such optimization is a challenging task, which eventually needs solving an inverse problem to find the best PC structure regardless of the possibility of fabrication, and it is beyond the scope of this paper. Instead, we used the figures of merit introduced in Section III to search among the well-known PC lattices for different sizes of air-holes, different polarizations, and other modifications that are fabrication-wise feasible to find the best “available” choice. Nevertheless, the same process can be extended to other geometries as well.

## VI. IMPLEMENTATION ISSUES

In the discussions so far, the concentration was on the demultiplexing behavior of the structure. In a practical implementation, however, there are other issues to be considered. Here, we list some of these issues briefly but a more extensive investigation of them is an open research topic.

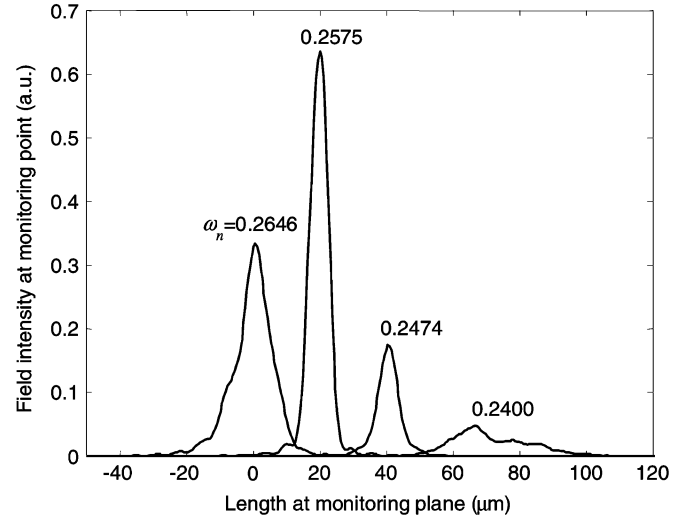


Fig. 5. Field intensities of four frequency channels at the output plane of the superprism-based demultiplexer designed in Fig. 4(a) are plotted. The PC consists of a 2-D square lattice of air-holes in Si, and TM polarization is assumed. The ratio of hole radius to lattice constant is  $r/a = 0.30$ , incident angle  $\alpha = 14^\circ$ , and  $\beta_{\text{opt}} = 2.44$ . The angular spacing between adjacent channels for  $X = -20 \text{ dB}$  is  $\Theta = 5.6^\circ$ , and input divergence angle is  $\Delta\alpha = 3.2^\circ$ . For this design, at  $\lambda = 1550 \text{ nm}$ , propagation length is  $L = 210 \mu\text{m}$ . The normalized center frequency of each channel is shown on top of its corresponding intensity profile.

1) *Reflection at the Interfaces of the Photonic Crystal Region:* Reflection at the boundaries of the device is one of the major issues in the implementation. It results in both loss of power and complications due to multiple passes of the beam through the structure. There have been proposals for reducing the reflection by modifying the layer at the interface [19] or by using a multilayer grating to provide mode matching [21], but a complete solution for reflection reduction at the interface still remains as one of the obstacles in practical realization of superprism-based demultiplexers.

2) *Polarization of the Beam:* The superprism-based demultiplexers discussed so far work for a specific polarization. Using these structures along with polarization-insensitive devices will add either more loss or more complexity in the design to account for the polarization using one of the standard methods.

3) *Input/Output Coupling Stages:* In order to match the field behavior inside the superprism-based demultiplexer to those in the input and output devices, use of coupling stages is almost inevitable. In general, there are three major tasks for an ideal coupling stage: 1) reducing the reflection by matching the fields at different regions; 2) diffraction compensation [18] to eliminate the broadening effects due to the propagation of the beams at the output and regenerating the beams with sizes consistent with output stages; and 3) providing the field in the appropriate polarization for which the demultiplexing stage is designed. For coupling of light into PC structures, some methods based on modification of the interface of the PC [19] and incorporating a diffraction grating input layer [21] have been recently proposed to reduce the reflection loss. A complete solution, however, is still a subject to be investigated in future.

4) *From 2-D to 3-D and Planar Structures:* All the structures we considered in this paper were 2-D structures. Although this gives us a reasonable starting point for the design, in the

actual design either in the form of planar structures (with finite thickness) or three-dimensional (3-D) periodic structures, other considerations come into the picture. For planar structures, the design has to satisfy confinement requirements in the third dimension. Also, even for in-plane propagation in this case, the bands are different from their 2-D counterparts. Therefore, the 2-D band structure for the in-plane propagation has to be calculated and used to optimize the structure for best demultiplexing performance. Nevertheless, the methods explained here (i.e., effective index model, performance measures, etc.) can be used once the corresponding band structure is calculated.

5) *Propagation Loss*: In designing planar PC structures, care must be taken in designing the structure in a region for which confinement in the third dimension is provided to avoid excessive loss. Even in these regions, in practice, due to fabrication imperfections, scattering is present and results in loss. The scattering loss in PC devices because of their large permittivity contrast is typically very large. Avoiding this loss is one of the driving forces for design of more compact structures. Recent development in fabrication facilities and methods has resulted in considerable loss reduction [25]. Nevertheless, making designs to be less sensitive to fabrication imperfections is a general issue for all PC structures, which needs more investigation and is beyond the scope of this paper.

## VII. CONCLUSION

The demultiplexing capability of superprism-based PC devices is revisited and procedure for designing these structures are presented. We have discussed different schemes for demultiplexing applications and performed an optimization for conventional PC lattices. Our results show that in most practical cases, triangular lattice PC of air-holes in Si substrate with TE polarization and interface along  $\Gamma M$  direction exhibits the best demultiplexing performance among well-known PC lattices. Using those results, a unified design process based on effective index model is provided which can be used to efficiently find parameters for conventional superprism-based demultiplexers for a range of different applications. We have also shown that extension of the same design process for a more practical planar PC structure is possible, and pointed out implementation issues for realization of these devices.

## REFERENCES

- [1] E. Yablonovitch, "Inhibited spontaneous emission in solid state physics and electronics," *Phys. Rev. Lett.*, vol. 58, pp. 2059–2062, May 1987.
- [2] S. John, "Strong localization of photons in certain disordered dielectric superlattices," *Phys. Rev. Lett.*, vol. 58, pp. 2486–2489, Jun. 1987.
- [3] E. Yablonovitch, "Photonic bandgap structures," *J. Opt. Soc. Amer. B*, vol. 10, pp. 283–295, 1993.
- [4] J. D. Joannopoulos, R. D. Meade, and J. N. Winn, *Photonic Crystals: Molding the Flow of Light*. Princeton, NJ: Princeton Univ. Press, 1995.
- [5] S. G. Johnson and J. D. Joannopoulos, "Designing synthetic optical media: Photonic crystals," *Acta Materialia*, vol. 51, pp. 5823–5835, 2003.
- [6] Sh.-Y. Lin, V. M. Hietala, L. Wang, and E. D. Jones, "Highly dispersive photonic bandgap prism," *Opt. Lett.*, vol. 21, pp. 1771–1773, Nov. 1996.
- [7] H. Kosaka, T. Kawashima, A. Tomita, M. Notomi, T. Tamamura, T. Sato, and S. Kawakami, "Superprism phenomena in photonic crystals," *Phys. Rev. B*, vol. 58, pp. R10096–R10099, Oct. 1998.

- [8] ———, "Superprism phenomena in photonic crystals: Toward microscale lightwave circuits," *J. Lightw. Technol.*, vol. 17, pp. 2032–2038, Nov. 1999.
- [9] K. B. Chung and S. W. Hong, "Wavelength demultiplexers based on the superprism phenomena in photonic crystals," *Appl. Phys. Lett.*, vol. 81, pp. 1549–1551, Aug. 2002.
- [10] T. Baba and T. Matsumoto, "Resolution of photonic crystal superprism," *Appl. Phys. Lett.*, vol. 81, pp. 2325–2327, Sep. 2002.
- [11] B. Momeni and A. Adibi, "Optimization of photonic crystal demultiplexers based on the superprism effect," *Appl. Phys. B*, vol. 77, pp. 555–560, Nov. 2003.
- [12] B. E. Nelson, M. Gerken, D. A. B. Miller, R. Piestun, C. C. Lin, and J. S. Harris Jr., "Use of a dielectric stack as a one-dimensional photonic crystal for wavelength demultiplexing by beam shifting," *Opt. Lett.*, vol. 25, pp. 1502–1504, Oct. 2000.
- [13] M. Gerken and D. A. B. Miller, "Multilayer thin-film structures with high spatial dispersion," *Appl. Opt.*, vol. 42, pp. 1330–1345, Mar. 2003.
- [14] L. Wu, M. Mazilu, T. Karle, and T. F. Krauss, "Superprism phenomena in planar photonic crystals," *IEEE J. Quantum Electron.*, vol. 38, no. 7, pp. 915–918, Jul. 2002.
- [15] A. I. Cabuz, E. Centeno, and D. Cassagne, "Superprism effect in bidimensional rectangular photonic crystals," *Appl. Phys. Lett.*, vol. 84, pp. 2031–2033, Mar. 2004.
- [16] B. Momeni and A. Adibi, "Controlling diffraction of optical beams using photonic crystals," in *Proc. SPIE, Photonic Crystal Materials Devices II*, vol. 5360, A. Adibi, A. Scherer, and S.-Y. Lin, Eds., Jul. 2004, pp. 355–363.
- [17] M. Notomi, "Theory of light propagation in strongly modulated photonic crystals: Refractionlike behavior in the vicinity of the photonic band gap," *Phys. Rev. B*, vol. 62, pp. 10696–10705, Oct. 2000.
- [18] B. Momeni and A. Adibi, "An approximate effective index model for efficient analysis and control of beam propagation effects in photonic crystals," *J. Lightwave Technol.*, vol. 23, no. 3, pp. 1522–1532, Mar. 2005.
- [19] T. Baba and D. Ohsaki, "Interfaces of photonic crystals for high efficiency light transmission," *Jpn. J. Appl. Phys.*, pt. 1, vol. 40, pp. 5920–5924, Oct. 2001.
- [20] T. Baba, T. Matsumoto, and M. Echizen, "Finite difference time domain study of high efficiency photonic crystal superprisms," *Opt. Express*, vol. 12, pp. 4608–4613, Sep. 2004.
- [21] J. Witzens, M. Hochberg, T. Baehr-Jones, and A. Scherer, "Mode matching interface for efficient coupling of light into planar photonic crystals," *Phys. Rev. E*, vol. 69, p. 046 609, Apr. 2004.
- [22] R. D. Meade, A. M. Rappe, K. D. Bromme, J. D. Joannopoulos, and O. L. Alerhand, "Accurate theoretical analysis of photonic bandgap materials," *Phys. Rev. B*, vol. 48, pp. 8434–8437, Sep. 1993.
- [23] A. Yariv and P. Yeh, *Optical Waves in Crystals: Propagation and Control of Laser Radiation*. New York: Wiley, 1984.
- [24] L. Wu, M. Mazilu, and T. F. Krauss, "Beam-steering in planar photonic crystals: From superprism to supercollimator," *J. Lightw. Technol.*, vol. 21, no. 2, pp. 561–566, Feb. 2003.
- [25] S. J. McNab, N. Moll, and Y. A. Vlasov, "Ultra-low loss photonic integrated circuit with membrane-type photonic crystal waveguides," *Opt. Express*, vol. 11, pp. 2927–2939, Nov. 2003.



**Babak Momeni** (S'02) was born in Tehran, Iran, in 1977. He received the B.Sc. and M.Sc. degrees in electrical engineering from Sharif University of Technology, Tehran, Iran, in 1999 and 2001, respectively. He is currently working towards the Ph.D. degree at the Georgia Institute of Technology, Atlanta.

His research interests include wave propagation in periodic structures, nonlinear optics, and resonance effects in electromagnetic structures.

Mr. Momeni is a member of the Optical Society of America (OSA) and the International Society for Optical Engineers (SPIE), Bellingham, WA, and Eta Kappa Nu.



**Ali Adibi** (M'00–SM'04) was born in Shiraz, Iran, in 1967. He received the B.S.E.E. degree from Shiraz University, Shiraz, in 1990, the M.S.E.E. degree from the Georgia Institute of Technology, Atlanta, in 1994, and the Ph.D. degree from the California Institute of Technology, Pasadena, in 1999. His Ph.D. research resulted in a breakthrough in persistent holographic storage in photorefractive crystals.

He worked as a Postdoctoral Scholar at the California Institute of Technology from 1999 to 2000. He has been an Assistant Professor in the School of Electrical and Computer Engineering, Georgia Institute of Technology, since 2000. His research interests include holographic data storage, holographic optical elements for optical communications, 3-D optical pattern recognition, design, characterization, and applications of photonic crystals for chip-scale WDM and biosensors, and optical communication and networking. He has been the Conference Chair for the Photonic Bandgap Materials and Devices Conference, PhotonicWest, since 2001, and the Program Chair for the Nanotechnology Program, PhotonicWest, since 2002.

Dr. Adibi is a member of Sigma Xi, OSA, SPIE, and the Materials Information Society (ASM). He has served as a Technical Committee Member for several conferences including the IEEE Lasers and Electro-Optics Society (LEOS) Annual Meeting. He has also been a Member of the Apker Award Selection Committee since 2002. He is the recipient of numerous awards including the Packard Fellowship (from the David and Lucile Packard Foundation), the National Science Foundation (NSF) Career Award, the Southeastern Center for Electrical Engineering Education (SCEEE) Young Faculty Development Award, the NASA Space Act Award, SPIE's Young Investigator Award, Howard Ector Outstanding Teacher Award from the Georgia Institute of Technology, the Richard M. Bass Outstanding Teacher Award from Georgia Institute of Technology, the Charles H. Wilts Prize for the best electrical engineering thesis of the year from the California Institute of Technology, the New Focus Student Award from the Optical Society of America (OSA), the Top Student (D. J. Lowell) Award from the International Society for Optical Engineering (SPIE), and the Oscar P. Cleaver Award for the Outstanding Electrical Engineering Graduate Student of the Year, from the Georgia Institute of Technology.